Eur. Phys. J. B **44**, 431–438 (2005)
DOI: 10.1140/epjb/e2005-00142-3

THE EUROPEAN PHYSICAL JOURNAL B

Spectroscopic ellipsometric evidence of the solid-state reactions in Ni/Si multilayered films, induced by ion-beam mixing and thermal annealing

Y.P. Lee[1,a], Y.V. Kudryavtsev[2], Y.N. Makogon[3], E.P. Pavlova[3], and J.Y. Rhee[4]

[1] Quantum Photonic Science Research Center and Department of Physics, Hanyang University, Seoul, 133-791 Korea
[2] Institute of Metal Physics, National Academy of Sciences of Ukraine, 36 Vernadsky str, 03142, Kiev-142, Ukraine
[3] NTU "Kiev Polytechnical Institute", 37 Pobedy ave., Kiev, Ukraine
[4] Department of Physics, Hoseo University, Asan, Choongnam 336-795, Korea

Received 27 March 2004
Published online 30 May 2005 –

Abstract. Solid-state reactions, induced by ion-beam mixing (IBM) and thermal annealing, in Ni/Si multilayered films (MLF) with an overall stoichiometry of Ni_2Si, NiSi and $NiSi_2$, while keeping the nominal thickness of Ni sublayer constant (3.0 nm), were studied by using spectroscopic ellipsometry as well as X-ray diffraction (XRD). The mixing was performed with Ar^+ ions of an energy of 80 keV and a dose of 1.5×10^{16} Ar^+/cm^2. Unlike the results of our previous study on Fe/Si MLF [Y.V. Kudryavtsev et al., Phys. Rev. B **65**, 104417 (2002)], it was shown that an amorphous phase of NiSi in the $B20$ phase was formed during deposition independent of the overall stoichiometry of MLF, i.e., the nominal thickness of Si sublayer. IBM leads to some structural changes in the Ni/Si MLF, which cannot be detected by XRD but are confidently recognized by optical tools. A thermal annealing at 673 K of the Ni/Si MLF with an overall stoichiometry of NiSi and $NiSi_2$ causes formation of the η-NiSi phase. The first trace of $NiSi_2$ phase on the background of the η-NiSi phase was detected by XRD after an annealing at 1073 K, while, according to the optical results, $NiSi_2$ turned out to be the dominant phase for the annealed Ni/Si MLF with an overall stoichiometry of $NiSi_2$.

PACS. 78.66.Bz Metals and metallic alloys – 78.67.Pt Multilayers; superlattices – 78.20.Bh Theory, models, and numerical simulation – 61.80.Jh Ion radiation effects

1 Introduction

Metal silicides play an important role in modern Si-based electronics. However, owing to a narrow compositional range for the silicide formation and to high melting points, processing of these intermetallics by the conventional methods is rather difficult. The ability to grow silicides on semiconductor materials in a more controlled manner has become increasingly important for the very-large-scale-integrated technology.

The Ni-Si system is characterized by the existence of several congruent (C) and nonconcongruent (NC) silicides [β-Ni_3Si (NC), γ-$Ni_{31}Si_{12}$ (C), δ-Ni_2Si (C), ϵ-Ni_3Si_2 (NC), η-NiSi (C) and $NiSi_2$ (NC)], all of which are stable at room temperature (RT) with a negative heat of formation of 36, 42, 48, 46, 45 and 31 kJ/mol, respectively [1]. From a thermodynamical point of view, the nickel silicide formation by thermal annealing of a Ni film deposited onto a Si wafer is a consequence of a decrease in the free energy through the reaction, and a certain external energy substantially accelerates the silicide formation by changing the thermodynamic energy of system.

Solid-state reactions between a Ni thin film and a Si substrate during annealing have been studied intensively [2–8]. Olowolafe et al. [2] were the first to show that the initial silicide phase, formed from a polycrystalline Ni film of 100 nm in thickness on a single crystalline Si substrate, is δ-Ni_2Si. The sequence of the nickel silicide phases depends on the first layered structure. Thus, for instance, a polycrystalline Ni film of 100−500 nm in thickness, deposited on a single-crystalline Si, first forms the δ-Ni_2Si phase upon annealing at 473−600 K; annealing at 873 K, however, leads to formation of the η-NiSi and the δ-Ni_2Si phases. The $NiSi_2$ phase is formed during an annealing at 1073 K [9]. Contrary to the aforementioned cases, the initial nickel silicide phase formed in a polycrystalline-Ni/amorphous-Si bilayer is amorphous NiSi, while the second one is a polycrystalline δ-Ni_2Si [4]. Bokhonov and

[a] e-mail: yplee@hanyang.ac.kr

Korchagin have also shown that the formation sequence of Ni-silicide phases is different for Ni deposited on single-crystalline and amorphous Si substrates [7].

Apparently "new" phenomena, in comparison with thick (∼100 nm or thicker) $3d$-transition-metal films deposited onto a Si wafer, can be observed in the following multilayered-film (MLF) structures: the sequential phases, the formation of metastable phases which are not identified in the equilibrium phase diagram [10], an extremely rapid growth (an "explosive" reaction) [4], the formation of amorphous interlayers by a reaction between the crystalline sublayers [11]. For example, it was shown that a metastable metallic iron monosilicide with CaF_2 type of structure was spontaneously formed in the interfacial regions of the Fe/Si MLF for the case of a nominal Si sublayer thicknesses of about 1−2 nm [12].

All the aforementioned Ni silicides exhibit noticeable negative heats of formation. Therefore, a multilayer structure can make the heat of formation released at all interfaces, which might result in the explosive formation of a Ni silicide. However, the explosive silicidation in Ni/Si multilayers has been observed only when the sublayer thickness was less than 12.5 nm and the MLF is free, i.e., detached from the substrate [4].

On the other hand, the employment of ion-beam mixing (IBM) for silicide formation can lead to the interaction between the two kinds of sublayers by the energetic incident ions in such a way that silicide formation can not be achieved by conventional equilibrium techniques. IBM comprises not only the energy to activate the interfacial interaction but also the diffusion necessary to maintain silicide growth. For example, IBM of Fe/Si MLF led to formation of the metastable Fe_2Si silicide with a $B2$-type structure and a rather perfect crystallininty [13]. An unusual distribution of Ni atoms was observed by Wu et al. [14] in NiSi structures formed by ion-beam synthesis (the Ni atoms were implanted into a Si wafer). It was also shown that the equilibrium phases of β-Ni_3Si, η-NiSi and $NiSi_2$ with unique morphologies can be formed at lower temperatures by irradiating a Ni-on-Si system by high-energy Xe ions [15]. Another formation sequence of Ni-silicide phases [amorphous NiSi → δ-Ni_2Si (due to an annealing at 473−573 K) → Ni_5Si_2 (due to an annealing at 573−673 K) → β-Ni_3Si at 673−873 K] was observed when Ni ions were implanted into a Si substrate [16].

The ability to predict a phase formation sequence and phase decomposition during solid-state reaction, reactive deposition and ion-beam mixing in terms of the effective-heat-of-formation model was illustrated by Pretorius et al. [17]. Nevertheless, in practice, in order to answer the question "*what product of the solid state reaction appears in the interfacial region of layered structures?*" experimental tools should be employed, which are sensitive to the local environment like nuclear magnetic resonance or Mössbauer spectroscopies in addition to the standard structural-analysis methods such as X-ray diffraction (XRD) or transmission-electron microscopy. In such a way a pioneering investigation on the phases formed in the interfacial regions of Fe/Si multilayers has been done by Decoster et al. [18] by employing Mössbauer spectroscopy. However, its use is restricted only to layers containing the Mössbauer isotopes or, in the case of nuclear magnetic resonance, to the systems with isotopes possessing nuclear magnetic moments. Contrary to aforementioned local-environment sensitive tools, the optical and magneto-optical (MO) spectroscopies are free from such constraints.

It is well known that both optical and MO properties of metals depend strongly on their electronic energy structures, which are correlated with the atomic and magnetic ordering. The interdiffusion between Ni and Si atoms in the Ni/Si MLF, induced by the IBM or by thermal annealing, should change the chemical and the atomic order in the reactive zone as well as decrease the thickness of pure-Ni sublayers (and hence, the magnetic and MO responses). Evidently, the real structures and the magnetic properties of the as-deposited and reacted MLF can be verified by a comparison between experimental and computer-simulated optical and MO data, based on an appropriate model for the structure of MLF and the properties of the constituent sublayers. The effectiveness of such an approach for the study of the crystallization of amorphous alloy films, based on the $3d$-transition metal, was demonstrated in reference [19]. It was shown that the nucleation of a new crystalline phase in the amorphous matrix of alloy was detected by optical tools earlier than by the conventional XRD methods. The optical properties of crystalline Ni-silicide films were investigated several times by using reflectivity [20,21] or spectroscopic ellipsometry [22,23]. These enable us to compare the optical properties of the reacted Ni/Si MLF with those of various crystalline silicides. Thus, this work aims to mainly employ optical and MO spectroscopies for a comprehensive study of the influence of ion-beam treatment and thermal annealing on the structure and the physical properties of Ni/Si MLF.

2 Experimental procedure

Several Ni/Si MLF have been prepared by dc-sputtering on single-crystalline Si substrates kept at room temperature (RT). The ratios of sublayer thicknesses in the Ni/Si MLF were chosen to obtain the overall stoichiometries of Ni_2Si, NiSi and $NiSi_2$. The topmost layer of all the Ni/Si MLF was always Ni. The nominal individual sublayer thicknesses were chosen in order to secure the individuality of sublayers and also to be thinner than the skin-penetration depth. Total MLF thickness should be also thick enough to avoid possible light reflection from the Si substrate The nominal and actual parameters of the prepared Ni/Si MLF are summarized in Table 1.

The structural characterization of Ni/Si MLF was performed by high-angle X-ray diffraction (HAXRD) and low-angle X-ray diffraction (LAXRD) with Co-K_α radiation. The HAXRD study has been made by using the Debye-Sherrer photographic camera. The magnetic state of the as-deposited Ni/Si MLF was checked by measuring the in-plane and the out-of-plane magnetization hysteresis

Table 1. Parameters of the prepared Ni/Si MLF. t_{Ni} and t_{Si} stand for the thicknesses of Ni and Si sublayers, respectively, and n is the number of bilayer repetitions.

	Nominal		n	Measured	
Sample no.	t_{Ni}/t_{Si} (nm/nm)	stoich.		t_{Ni}/t_{Si} (nm/nm)	stoich.
1	3.0/2.69	Ni_2Si	40	4.3/3.9	$Ni_{0.67}Si_{0.33}$
2	3.0/5.37	NiSi	50	3.65/6.75	$Ni_{0.50}Si_{0.50}$
3	3.0/10.7	$NiSi_2$	22	3.9/13.9	$Ni_{0.35}Si_{0.65}$

loops, $M(H)$, at RT by using a vibrating-sample magnetometer (VSM).

The optical properties [optical conductivity (OC: $\sigma = \varepsilon_2 \times \omega/4\pi$), where ε_2 is the imaginary part of the diagonal components of the dielectric tensor $\widetilde{\varepsilon}_{xx} = \widetilde{\varepsilon}_{yy} = \widetilde{\varepsilon}_{zz} = \varepsilon = \varepsilon_1 - i\varepsilon_2$], of the as-deposited and post-treated Ni/Si MLF were studied at RT by spectroscopic ellipsometry. The details of the optical and the MO [equatorial Kerr effect (EKE)] measurements can be found elsewhere [24].

After the structural and physical properties of the as-deposited Ni/Si MLF were investigated, the MLF were ion-beam mixed in a high vacuum ($\sim 1 \times 10^{-6}$ Torr) by Ar^+ ions directed normally to the film surface at the following conditions: an ion energy of 80 keV, an ion flux of 1.5×10^{-6} A/cm^2, and an ion dose of 1.5×10^{16} Ar^+/cm^2. After the mixing all the measurements were repeated. Besides IBM, thermal annealing at 473, 673, 873 and 1073 K, was also employed to the as-deposited Ni/Si MLF. After each step of annealing the structural and physical properties of Ni/Si MLF were studied again.

The simulation of the optical and the MO properties of Ni/Si MLF was performed by exactly solving the multiple-reflection problem using the scattering matrix approach [25]. The simulation needs theoptical and MO properties of the constituent sublayers of Ni/Si MLF as input parameters for the simulation. For this purpose, pure polycrystalline Ni and amorphous Si films of 100 and 650 nm in thickness, respectively, were deposited at the same conditions and their optical and MO properties were investigated at RT.

3 Results and discussion

We were not able to observe any visible rings in the HAXRD patterns for all the as-deposited Ni/Si MLF (see Figs. 1 and 2). The dots in Figures 1 and 2 are all substrate related. The lack of diffraction lines on the HAXRD patterns might be understood as the formation of an amorphous-like structure in the Ni/Si MLF due to a solid-state reaction [11], or as a short coherence length in crystalline sublayers in the Ni/Si MLF. However, such an amorphous-like structure is not homogeneous, since the corresponding LAXRD patterns exhibit several well-defined satellites which indicates their layered structure

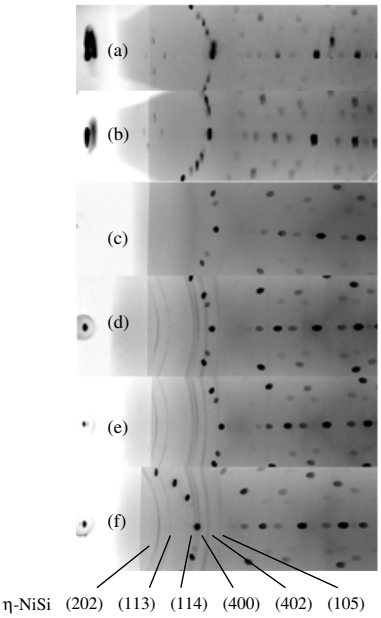

Fig. 1. High-angle XRD patterns for (a) the as-deposited, (b) the ion-beam mixed and annealed [at (c) 473 K, (d) 673 K, (e) 873 K and (f) 1073 K] (3.65 nm Ni/6.75 nm Si)$_{50}$ MLF.

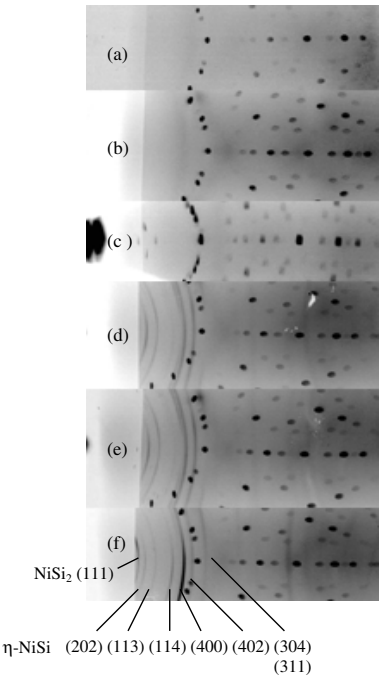

Fig. 2. The same as Figure1, except for (3.9 nm Ni/13.9 nm Si)$_{22}$ MLF.

(see Fig. 3). The actual modulation lengths (or the bilayer periods), Λ, for the as-deposited Ni/Si MLF were calculated to be 8.2, 10.4 and 17.8 nm for the samples 1, 2 and 3, respectively.

The magnetic properties of the as-deposited Ni/Si MLF look rather unusual. The in-plane and the out-of-plane $M(H)$ loops (not shown) exhibit features of superparamagnetic behavior and practically coincide

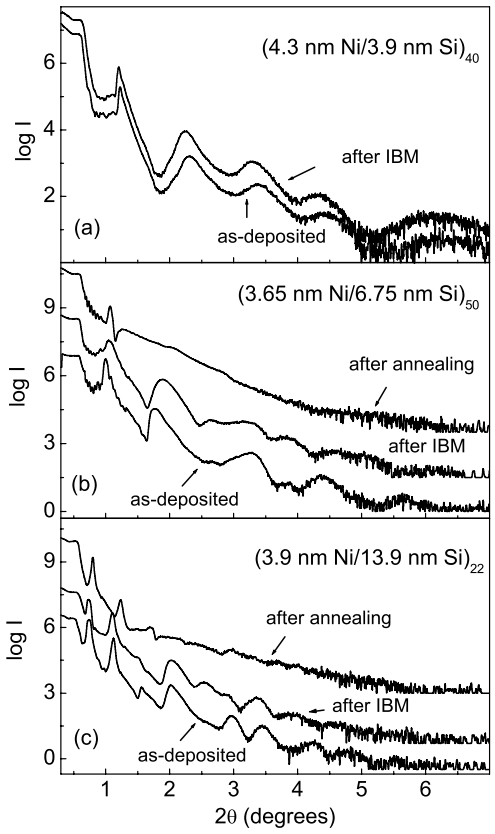

Fig. 3. Low-angle XRD spectra for the as-deposited, the ion-beam mixed and the annealed (at 1073 K) (a) (4.3 nm Ni/3.9 nm Si)$_{40}$, (b) (3.65 nm Ni/6.75 nm Si)$_{50}$ and (c) (3.9 nm Ni/13.9 nm Si)$_{22}$ MLF.

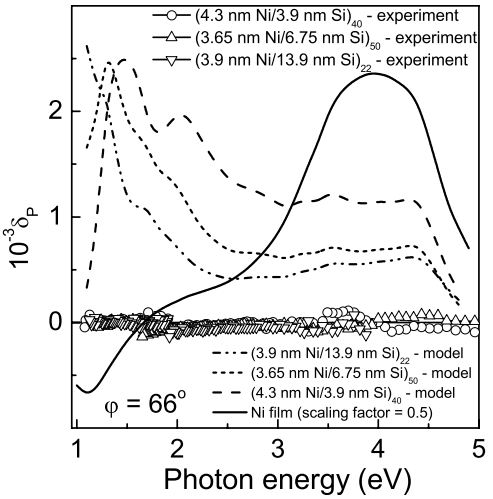

Fig. 4. Experimental and simulated EKE spectra for Ni/Si MLF and Ni film.

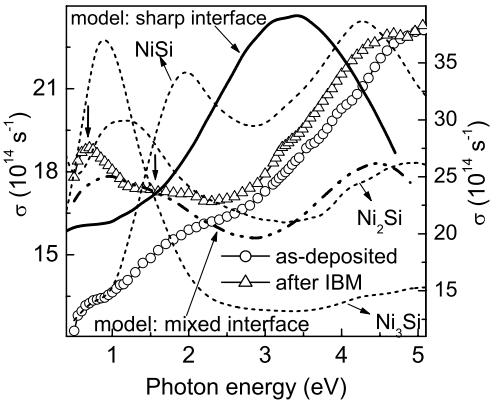

Fig. 5. Experimental OC spectra for the as-deposited and the ion-beam mixed (4.3 nm Ni/3.9 nm Si)$_{40}$ MLF (left scale). Modelled OC spectrum for this MLF, together with the literature data for NiSi, Ni_2Si and Ni_3Si (Ref. [20]) are also shown for comparison (right scale). OC spectrum for Ni_3Si is shown with a scaling factor of 0.65.

with each other. A rapid loss of the magnetic order in Ni upon alloying with Si was mentioned by Babu et al.: above a critical composition of about 13 at.% Si, the magnetic order is absent at a nonzero temperature [27]. Thus, according to the magnetic results it is natural to assume a superparamagnetic behavior owing to the Ni sublayer enrichment by Si.

Such data, obtained by VSM, also corroborate the results of MO measurements. The experimental MO responses for all the as-deposited Ni/Si MLF are extremely weak (or simply absent), and are drastically smaller than the simulated ones, based on an MLF model with sharp interfaces between sublayers of measured thicknesses (see Fig. 4). The MO results also enable us to conclude that the actual structure of the as-deposited Ni/Si MLF are significantly different from the simulated one. In order to explain this, it should also be assumed that Ni sublayers lost their ferromagnetic order owing to their enrichment by Si (at least up to 13 at.% of Si).

The OC spectra for the as-deposited Ni/Si MLF with relatively thin Si sublayers and overall stoichiometries of Ni_2Si and NiSi exhibit a gradual increase in magnitude with increasing photon energy, showing a feature at $\hbar\omega \approx 2$ eV (see Figs. 5 and 6). Contrary to the aforementioned Ni/Si MLF, the OC spectrum for the as-deposited (3.9 nm Ni/13.9 nm Si)$_{22}$ MLF shows a prominent absorption peak at about 3.3 eV (see Fig. 7). In order to understand the experimentally observed optical properties of the as-deposited Ni/Si MLF, a comparison with the simulated ones was performed.

The optical properties of amorphous Si as well as polycrystalline Ni have been well investigated [29–31]. Thus, it is well known that the OC spectrum for amorphous Si films exhibits a very intense absorption peak near 3.9 eV, and shows a rather rapid (nearly down to zero) decrease in the magnitude with decreasing photon energy. The OC spectrum of Ni is characterized by the main absorption peak at 4.5 $\sim$ 4.7 eV and a gradual increase in magnitude with decreasing photon energy for an energy range of $\hbar\omega < 3$ eV. The experimental spectra of our Ni and Si films are in good agreement with literature data. The simulated OC spectra for all the Ni/Si MLF look similar to each other, exhibiting a

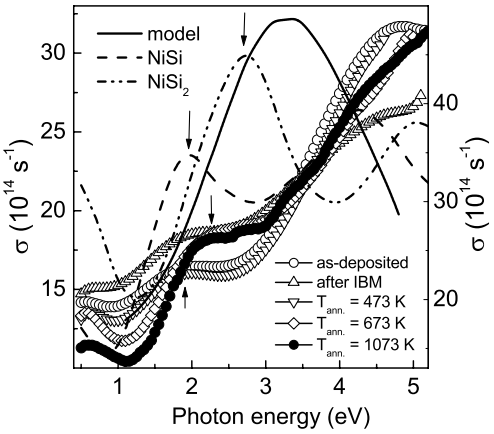

Fig. 6. Experimental OC spectra for the as-deposited, the ion-beam mixed and the annealed [at 473 K, 673 K and 1073 K] (3.65 nm Ni/6.75 nm Si)$_{50}$ MLF (left scale). Modelled OC spectrum for this MLF, together with the literature data for NiSi and $NiSi_2$ (Ref. [20]) are also shown for comparison (right scale).

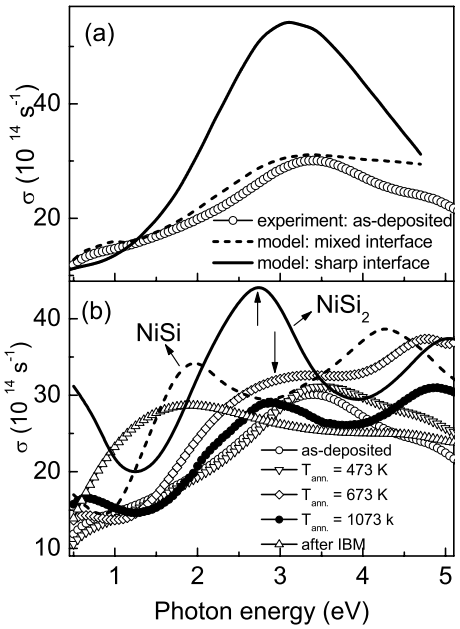

Fig. 7. Experimental OC spectra for the (a) as-deposited, and (b) the ion-beam mixed and the annealed [at 473 K, 673 K and 1073 K] (3.9 nm Ni/13.9 nm Si)$_{22}$ MLF together with the literature data for NiSi and $NiSi_2$ (Ref. [20]) are also shown for comparison. Modelled OC spectrum for this MLF obtained for different models are shown in panel (a).

prominent absorption peak near 3.1−3.3 eV (which evidently originates from the Si subalyers) and insignificant differences in the magnitude and peak locations (see Figs. 5−7). The absence of even any visible trace for this absorption peak in the experimental OC spectra of the as-deposited Ni/Si MLF with overall stoichiometries of Ni_2Si and NiSi enables us to suppose that the lack (or a noticeable reduction) of pure Si content in such films is due to the Si (and naturally the Ni) consumption for the Ni-silicide formation. This is consistent with Clevenger and Thompson: the employment of the destructive cross-sectional transmission electron microscopy allowed them to show that in the as-deposited Ni/Si MLF, an amorphous NiSi phase of about 4 nm in thickness is formed between polycrystalline Ni and amorphous Si sublayers [32]. It is also seen that reasonable correspondence in the shape between the simulated and experimental OC spectra is observed only for the Ni/Si MLF with the thickest (among the investigated Ni/Si MLF) Si sublayers (see Fig. 7). However, the magnitude of the modelled OC spectrum is larger than that of the experimental one. Thus, we can conclude that the employed MLF model, assuming abrupt interfaces between pure Ni and Si sublayers and using the measured sublayer thicknesses (see Tab. 1), does not adequately describe the actual MLF structures.

The agreement between the simulated and experimental OC spectra of the as-deposited (3.9 nm Ni/13.9 nm Si)$_{22}$ MLF is significantly improved in spectral shape and magnitude if the complete consumption of the Ni sublayers and hence a noticeable part of the Si sublayers, to form nonferromagnetic Ni-silicides of NiSi and Ni_3Si stoichiometries. In this case, the (3.9 nm Ni/13.9 nm Si)$_{22}$ MLF's structure should be substituted in the simplified model by the (5.2 nm NiSi/1.4 nm Ni_3Si/5.6 nm Si/5.2 nm NiSi)$_{22}$ one (see Fig. 7). As input parameters for Ni_3Si and amorphous NiSi, the literature results for crystalline Ni_3Si [20] as well as our experimental data for the as-deposited (3.65 nm Ni/6.75 nm Si)$_{50}$ MLF were used, since the latter one was measured to have a stoichiometry of NiSi. Thus, it is clear that the obtained optical results for the as-deposited Ni/Si MLF also agree qualitatively with the magnetic and MO results.

IBM does not produce any visible changes in the HAXRD patterns, or the LAXRD spectra of Ni/Si MLF (see Figs. 1−3). However, noticeable changes were observed in the OC spectra. The OC spectrum of the ion-beam mixed (4.3 nm Ni/3.9 nm Si)$_{40}$ MLF shows a prominent enhancement in magnitude for $\hbar\omega < 2.8$ eV, clearly revealing new absorption peaks at $\hbar\omega \sim 0.7$ and 1.8 eV (marked by arrows in Fig. 5). A comparison of the OC spectrum with those of various crystalline Ni silicides allows us to assume that the peak at ∼1.8 eV is probably related to the low-energy peak in the OC spectrum of crystalline NiSi, while the 0.7 eV one originates from Ni_2Si or, more probably, from Ni_3Si. This supposition is further supported by the comparison of the experimental OC spectra with the simulated one made for the model with alloyed interfacial region or mixed interface (MI) model (see Fig. 5). In this model the following periodic element of the (4.3 nm Ni/3.9 nm Si)$_{40}$ MLF was used: (3.0 nm Ni/0.3 nm Ni_3Si /4.6 nm NiSi/0.3 nm Ni_3Si). As input parameters for simulation the optical constants for crystalline Ni_3Si [20] and as-deposited Ni/Si MLF of NiSi stoichiometry were used. Thus, according to the optical results, IBM produces in the (4.3 nm Ni/3.9 nm Si)$_{40}$ MLF regions with a short-range order close to the crystalline NiSi and Ni_3Si. The prominent changes in the OC spectra, induced by IBM,

were also observed for the (3.9 nm Ni/13.9 nm Si)$_{22}$ MLF which could be interpreted in terms of a formation of structures with a short-range order close to NiSi (compare the corresponding OC spectra in Fig. 7).

Contrary to the aforementioned Ni/Si MLF, IBM does not produce any visible change in the OC spectrum of (3.65 nm Ni/6.75 nm Si)$_{50}$ MLF with an overall stoichiometry of NiSi: the spectrum after IBM (as well as as-deposited Ni/Si MLF) shows a peculiarity (or an absorption peak) at $\hbar\omega \approx 2$ eV. Such a peak is absent in the OC spectra of pure Ni and Si, but present in that of crystalline NiSi (see Fig. 6). Clevenger and Thompson revealed the experimental and thermodynamical evidences that the reaction phase selection in a polycrystalline Ni/amorphous Si thin film is governed by the so-called "nucleation model": the formed silicide phase is one with the highest nucleation rate or the smallest nucleation barrier [32]. Therefore, it can be assumed that the nuclei of NiSi phase (for example, amorphous NiSi) are spontaneously formed during the deposition of (3.65 nm Ni/6.75 nm Si)$_{50}$ MLF, and IBM does not produce new ones.

Several explanations for the different sensitivities of the XRD and optical tools concerning the detection of the structural changes in the Ni/Si MLF induced by IBM may be proposed. The Ar^+-ion penetration depth (which is nearly equal to the mixing depth [28]), calculated in our previous work for the same mixing conditions for Fe/Si MLF, was 110 nm [13]. Assuming the same mixing depth for the Ni/Si MLF, we have to conclude that such IBM affects only the surface layers of Ni/Si MLF, keeping more than a half of the MLF volume undisturbed. This fact might explain the unchanged HAXRD and LAXRD patterns. At the same time, main features of the energy band structures of metals are determined by their short range orders, i.e. by the region of about $1.0 \sim 1.5$ nm in dimensions, while the coherence length for the formation of the detectable diffraction peak should be at least two times larger.

According to the HAXRD results, annealing at 473 K of the Ni/Si MLF does not induce any noticeable change in the MLF structure (see Figs. 1 and 2). Nearly the same conclusion can also be made on the basis of optical study: OC spectra for as-deposited and annealed at 473 K the samples 2 and 3 practically coincide with each other (see Figs. 6 and 7).

The first changes in the HAXRD pattern for the samples 2 and 3 begin to appear after an annealing at 673 K, indicating the formation of η-NiSi phase. Further increases in the annealing temperature to 873 K and 1073 K for the (3.65 nm Ni/6.75 nm Si)$_{50}$ MLF (sample 2) with an overall stoichiometry of NiSi does not cause any difference in the HAXRD pattern (see Fig. 1). In contrast to sample 2, an annealing at 1073 K of the (3.9 nm Ni/13.9 nm Si)$_{22}$ MLF (sample 3) with an overall stoichiometry of $NiSi_2$ leads to appearance (beside the diffraction lines for the η-NiSi phase) of the only (111) diffraction line for the $NiSi_2$ phase (see Fig. 2). Annealing at 1073 K of the (3.65 nm Ni/6.75 nm Si)$_{50}$MLF is accompanied by disappearance of the satellites in the LAXRD spectrum (except for the 1st-order satellite) and hence of the layered structure in this MLF (see Fig. 3). Contrary to the sample 2, the LAXRD spectrum for the sample 3 after an annealing at 1073 K still preserves weak traces of the satellites. This agrees with the HAXRD results: a two-phase structure of the annealed sample 3, indicating a composition gradient in the MLF. Thus, according to the HAXRD (and partly, the LAXRD) results, the (3.65 nm Ni/6.75 nm Si)$_{50}$ MLF is crystallized into the η-NiSi phase, while the annealing at 1073 K of the (3.9 nm Ni/13.9 nm Si)$_{22}$ MLF leads to the formation of a dual structure (a mixture of η-NiSi and $NiSi_2$) with a predominance of the η phase. It should be mentioned here that the observed sequence of the Ni-silicide phases, induced by the thermal annealing, in the investigated Ni/Si MLF differs from those in the literatures: an annealing at 1073 K of the Ni/Si layered structure usually leads to the $NiSi_2$ phase [5,7,8].

Thermal annealing at different temperatures (above 473 K) of the (3.65 nm Ni/6.75 nm Si)$_{50}$ causes gradual changes in the optical properties towards those of the crystalline NiSi: each step of annealing makes the interband absorption peak at $\hbar\omega \approx 2$ eV more evident. This means that such a process illustrates an improvement in the crystallininty of the NiSi phase. However, this is also accompanied by the blue-shift of the peak by about 0.2 eV. The comparison of the OC spectrum for the annealed (3.65 nm Ni/6.75 nm Si)$_{50}$ MLF at 1073 K with that of the crystalline $NiSi_2$ allows us to suppose that this shift is due to the formation of a certain amount of $NiSi_2$ phase in the annealed MLF. This assumption, however, is not supported by our HAXRD results, but is in the formation sequence for Ni silicides in the literatures.

Contrary to the HAXRD results, the evolution of the OC spectrum, induced by thermal annealing of the (3.9 nm Ni/13.9 nm Si)$_{22}$ MLF above 473 K, clearly indicates the formation of $NiSi_2$ phase (compare the OC spectrum for $NiSi_2$ and that of MLF after the annealing at 1073 K in Fig. 7). The experimental tools in this work have different probing depths (XRD and VSM – full film thickness, IBM - about 110 nm, optical and MO tool – about 20 nm). All of them play complementary roles in this study. The discrepancy between the results obtained by different experimental tools may indicate inhomogeneous processes in such complicated structures as MLF subjected to IBM or thermal annealing. Thus, the optical and HAXRD results might be correlated when we take into account the fact that the skin depth for the visible region is about 20 nm and also that the formation of $NiSi_2$ phase takes place mainly in the surface region of MLF, while the HAXRD response is made from the total volume of MLF.

The initial-stage Ni-silicide formation in the Ni/Si MLF during deposition is different from that of Fe/Si MLF. In our previous study on the Fe/Si MLF [13] we prepared only a pair of Fe/Si MLF, whose overall stoichiometry corresponds to Fe_2Si, with similar nominal sublayer thickness to check the reproducibility and the as-deposited Fe/Si MLF possesses crystalline layers

whose actual bilayer structure can be depicted as FeSi/Fe MLF, indicating a complete consumption of Si sublayer during the deposition owing to the Fe silicide formation. In this work we prepared three different MLF with the overall stoichiometry of Ni_2Si, NiSi and $NiSi_2$ to more systematically study the consumption of Si sublayer during the deposition owing to the initial-stage Ni-silicide formation. Indeed, it was confirmed that the Si sublayer was completely consumed for the Ni-rich Ni/Si MLF. For the case of Fe/Si MLF, a metastable $B2$-phase FeSi was formed at the interface during deposition, ensuring the antiferromagnetic coupling between Fe sublayers. Meanwhile, for the case of Ni/Si MLF, an almost amorphous phase, but close to the $B20$ phase, of NiSi was formed during deposition independent of the overall stoichiometry of MLF, i.e., the nominal thickness of Si sublayer.

4 Summary

1. The comparison of experimental and modelled optical properties of all the investigated Ni/Si MLF enables us to conclude that an amorphous region with a stoichiometry close to NiSi in the $B20$ phase is spontaneously formed during the deposition of MLF, independent of the nominal thickness of the Si sublayer. It is different from the case of Fe/Si MLF where a nonmagnetic crystalline metallic $B2$-phase FeSi, which is crucial to the antiferromagnetic coupling between Fe sublayers, is spontaneously formed. The thickness of such a region for the (3.9 nm Ni/13.9 nm Si)$_{22}$ MLF was estimated to be about 10 nm.

2. IBM of all the investigated Ni/Si MLF with overall stoichiometries of Ni_2Si, NiSi and $NiSi_2$ leads to the formation of regions with a shot-range order of the crystalline NiSi silicide, and of Ni_2Si (and/or Ni_3Si) additionally for the Ni/Si MLF with an overall stoichiometry of Ni_2Si.

3. An annealing at 1073 K of the as-deposited Ni/Si MLF destroys the layered structure of films and, according to the optical results, induces the formation of predominantly the η-NiSi phase for the (3.65 nm Ni/6.75 nm Si)$_{50}$ MLF and $NiSi_2$ for the (3.9 nm Ni/13.9 nm Si)$_{22}$ MLF.

4. The formation sequence for the Ni-silicide phases, determined by the optical and the structural methods, was found to be slightly different. Such a discrepancy can be explained when an inhomogeneous phase along the depth is formed.

5. The application of the optical tools to the study of solid-state reactions in Ni/Si MLF allowed us to identify the structural transformation, induced by IBM or thermal annealing, which were not detected by the traditional XRD method. We think that the differences in sensitivities is connected not with the difference in the probing depth, but with basic conditions for the formation of X-ray diffracted beam and main features of the energy band structures.

This work was supported by the KOSEF through Quantum Photonic Science Research Center (q-Psi), by Korea Research Foundation grant (KRF-01-015-DS0015), and by the MOST, Korea. We are also grateful to B. Szymański for his help in the XRD measurements, to T.I. Verbitskaya and D.L. Beke for the sample preparation, and to Y.N. Troshchenkov for the VSM measurements.

References

1. T.B. Massalski, *Binary Alloy Phase Diagram*, 2nd edn. (ASM, Metals Park, OH, 1990), Vol. 3, p. 2859
2. J.O. Olowolafe, M.-A. Nicolet, J.W. Mayer, Thin Solid Films **38**, 143 (1976)
3. S.P. Murarka, *Silicides for VLSI Applications* (Academic, Orlando, 1983)
4. L.A. Clevenger, C.V. Thompson, R.C. Cammarata, K.N. Tu, Appl. Phys. Lett. **52**, 795 (1988)
5. C.J. Tsai, K.H. Yu, Thin Solid Films **350**, 91 (1999)
6. P. Knauth, A. Charaï, C. Bergman, P. Gas, J. Appl. Phys. **76**, 5195 (1994)
7. B. Bokhonov, M. Korchagin, J. Alloys Comp. **319**, 187 (2001)
8. B.A. Julies, D. Knoesen, R. Pretorius, D. Adams, Thin Solid Films **347**, 201 (1999)
9. D. Mangelinck, P. Gas, A. Grob, B. Pichaud, O. Thomas, J. Appl. Phys. **79**, 4078 (1996)
10. E.E. Fullerton, J.E. Mattson, S.R. Lee, C.H. Sowers, Y.Y. Huang, G. Felcher, S.D. Bader, F.T. Parker, J. Magn. Magn. Mater. **117**, L301 (1992); G.J. Strijkers, J.T. Kohlhepp, H.J.M. Swagten, W.J.M. de Jonge, Phys. Rev. B **60**, 9583 (1999)
11. M.A. Hollander, B.J. Thijsse, E.J. Mittemeijer, Phys. Rev. B **42**, 5481 (1990)
12. A. Chaiken, R.P. Michel, M.A. Wall, Phys. Rev. B **53**, 5518 (1995)
13. Y.V. Kudryavtsev, Y.P. Lee, J. Dubowik, B. Szymański, J.Y. Rhee, Phys. Rev. B **65**, 104417 (2002)
14. M.F. Wu, J.D. Wachter, A.-M. Van Bavel, R. Moons, A. Vantomme, H. Pattyn, G. Langouche, H. Bender, J. Vanhellemont, K. Temst, Y. Bryunseraede, J. Appl. Phys. **78**, 1707 (1995)
15. O. Fathy, O.W. Holland, J. Narayan, J. Appl. Phys. **58**, 297 (1985)
16. Z. Rao, J.S. Williams, A.P. Pogany, D.K. Sood, G.A. Collins, J. Appl. Phys. **77**, 3782 (1995)
17. R. Pretorius, C.C. Theron, A.C. Vantomme, J.W. Mayer, Critical Reviews in Solid State and Material Sciences **24**, 1 (1999)
18. J. Decoster, H. Bemelmans, S. Degroote, R. Moons, J. Verheyden, A. Vantomme, G. Langouche, J. Appl. Phys. **81**, 5349 (1997)
19. B.P. Voznyuk, R. Gontarz, J. Dubowik, Yu.V. Kudryavtsev, N.A. Lesnik, Sov. Phys. Solid State. **32**, 409 (1990)
20. M. Amiotti, A. Borghesi, G. Guizetti, F. Nava, Phys. Rev. B **42**, 8939 (1990)
21. A. Humbert, A. Cros, J. Phys. Lett. **44**, L929 (1983)
22. H.W. Chen, J.T. Lue, J. Appl. Phys. **59**, 2165 (1986)

23. J.R. Jimenez, Z.C. Wu, L.J. Schowalter, B.D. Hunt, R.W. Fathauer, P.J. Grunthaner, T.L. Lin, J. Appl. Phys. **66**, 2738 (1989)
24. Y.P. Lee, K.W. Kim, Y.V. Kudryavtsev, V.V. Nemoshkalenko, B. Szymański, Eur. Phys. J. B **26**, 41 (2002)
25. R.M.A. Azzam, N.M. Bashara, *Ellipsometry and Polarized Light* (North-Holland, Amsterdam, 1977)
26. J. Kohlhepp, M. Valkier, A. van der Graaf, F.J.A. den Broeder, Phys. Rev. B **55**, R 696 (1997)
27. V.S. Babu, A.S. Pavlovic, M.S. Seehra, J. Appl. Phys. **79**, 5230 (1996)
28. G.S. Chang, S.M. Jung, J.H. Song, H.B. Kim, J.J. Woo, D.H. Byun, C.N. Whang, Nucl. Instr. Meth. B **121**, 244 (1997)
29. U. Schmid, J. Humliček, F. Lukeš, M. Cardona, U. Presting, H. Kibbel, E. Kaspar, K. Eberl, W. Wegscheider, G. Abstreiter, Phys. Rev. B **45**, 6793 (1992)
30. H. Ehrenreich, H.P. Philipp, D.J. Olechna, Phys. Rev. **131**, 2469 (1963)
31. M. Shiga, G.P. Pells, J. Phys. C **2**, 1847 (1969)
32. L.A. Clevenger, C.V. Thompson, J. Appl. Phys. **67**, 1325 (1990)